EPFL

Pollutant Transport in Urban Canyons

Course of *Environmental Transport Phenomena*

Matteo Calafà
Paolo Motta
Anna Peruso

Introduction

An urban canyon (also known as street canyon) is a place where the street is flanked by buildings on both sides creating a canyon-like environment. Typical examples are found in big American cities, as shown in Figure 1a[1]. The *street canyon effect*, *i.e.* the modification of the atmospheric boundary layer by the presence of an urban canyon, can affect temperature, wind speed and wind direction, amongst other. Its study is then crucial in order to improve urban human life. In particular, the aim of this project is to investigate differences in wind velocity profile and vehicles pollution transport in two different settings of an urban canyon: high-rise buildings and low-rise buildings. The latter could refer to Swiss towns, which are characterized by moderately short buildings (approximately 50 m), while the former can be associated to American cities, where it is possible to observe a high density of skyscrapers and very tall buildings, sometimes beyond 400 m. In order to simplify both the configurations, for each case study only a street with two rows of buildings is taken into consideration and one single road amidst. In addition, a perpendicular section to the street will be considered, in order to have a 2D formulation. Regarding the boundary conditions, wind is blowing perpendicularly to the street and pollution has its source at the bottom of the road (where vehicles are supposed to transit). In Figure 1b, a representation of our case study is shown.
Despite the simplification of the configuration, key elements of urban pollutant transport phenomena are to be observed: *canyon vortexes*, *pollution upward transport*, *mean wind covering effect*. In particular, for what mainly concerns our research, we expect to observe a more evident pollutant circulation in the low-buildings scenario as compared to the other one.

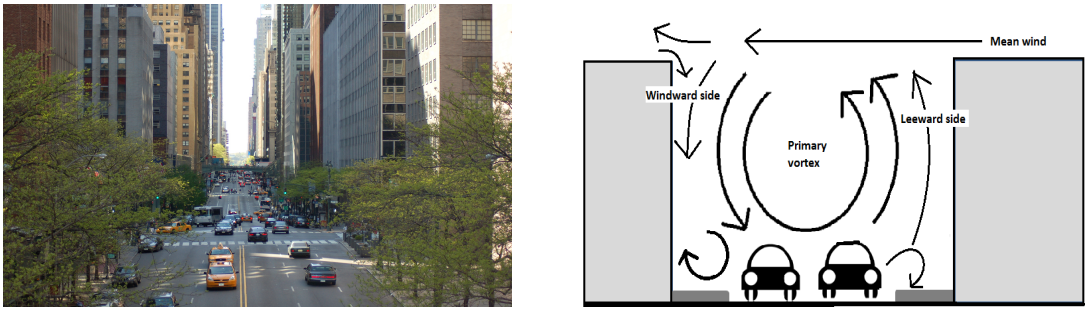

(a) Urban canyon in Manhattan. **(b)** 2-Dimensional Urban Canyon.

Figure 1: Case study.

1 Geometries and meshes

1.1 Low-rise morphologies

As previously mentioned, Swiss towns are typically made of short buildings. Hence, this problem geometry is characterized by buildings 50 m tall and 30 m wide. The street width is set to 25 m. All these dimensions are scaled by a factor of 100 in order to reduce the computational effort. First of all, we define D_x as the horizontal reference length that, for this domain, is the sum of the buildings and street widths ($D_x = 0.3 + 0.3 + 0.25 = 0.85\,m$). Then, the upstream domain length is $5D_x = 4.25\,m$, whereas the downstream domain length is $10D_x = 8.50\,m$. Finally, the whole domain height is fixed to $5D_x \approx 5\,m$. Although the block of buildings is the main area of interest, the domain is chosen so that the full development of the flow field can be observed. These simulations, indeed, require a sufficiently large domain size to minimize the effects of the artificial boundary conditions at the domain faces on the solution. However, placing the boundaries too far certainly increases the computational cost of the model, therefore it is important to select an optimal compromise. The domain for the low-rise buildings setting is shown in Figure 2.

[1]By David Brooks - https://www.flickr.com/photos/dpriddy/140684847/, CC BY 2.0, https://commons.wikimedia.org/w/index.php?curid=23159606

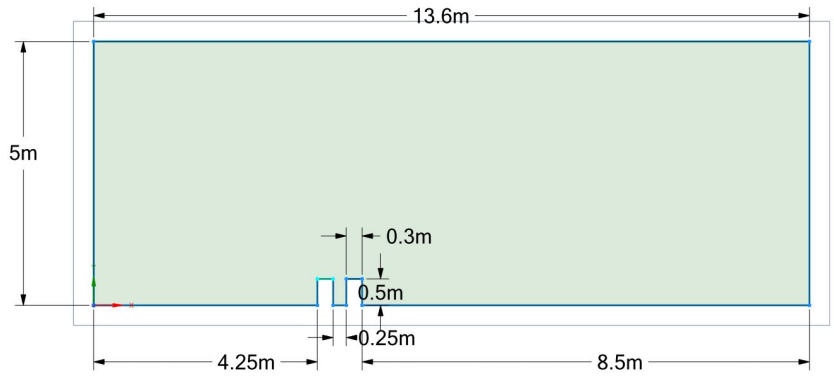

Figure 2: Low-rise domain geometry.

1.2 High-rise morphologies

In order to investigate the second case study, we need both to change the buildings size and their distance from inlet, outlet and top of the domain. In particular, the buildings widths are indeed $0.3\,m$ as before while the road width is $0.4\,m$. Here the reference value is the buildings height, $D_y = 4\,m$, this being the biggest dimension of the buildings block. Thus, upstream domain length is $3D_y = 12\,m$ and the downstream domain length is $5D_y = 20\,m$. The height of the domain is $4D_y = 16\,m$. For the high-rise buildings scenario, the domain is shown in Figure 3. Finally, all the described parameters are summed up in Table 1.

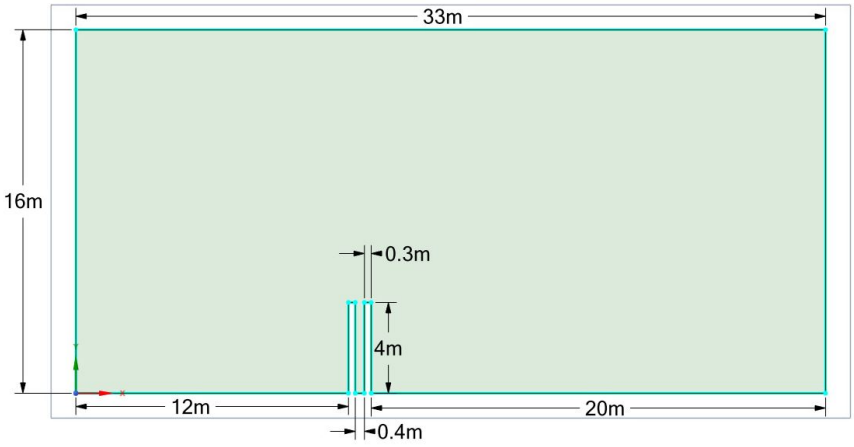

Figure 3: High-rise domain geometry.

	Low-rise m	High-rise m
Buildings height	0.5	4
Buildings width	0.3	0.3
Canyon width	0.25	0.4
Upstream width	4.25	12
Downstream width	8.5	20
Domain height	5	16

Table 1: Geometry parameters.

The dimensions of the computational domain are inferred from some recent results (see, for instance, [1]). However, most of the existing guidelines were found to be overly conservative when applied to tall buildings and the domain size used for this project turned out to be suitable for the presented simpler scenario.

1.3 Mesh

The next step of a CFD model consists of the discretization of the domain using a grid. Hence, it is necessary to define a mesh, that is the set of points where equations are solved. Since the project goal is to study the flow behaviour around the buildings, here a mesh with higher resolution will be needed. Moreover, in the same region, velocity and pressure gradients may be very high, requiring again a fine mesh. On the other hand, more regular solutions are expected to be found far from obstacles and here a coarser mesh suffices. In conclusion, an unstructured mesh (a grid with irregular topology) has been chosen for both domains (properties are shown in Table 2).

Ansys® parameter	Value
Edge-sizing (buildings)	$5 \cdot 10^{-3}\, m$
Edge-sizing (outer domain)	$0.1\, m$
Element size (mesh)	$0.2\, m$
Growth rate	1.05

Table 2: Mesh parameters.

Specifically, *edge-sizing* is the edge length of the elements on the domain boundary, *element size* is the maximum element size in the whole domain and *growth rate* represents the increase in element edge length with each succeeding layer of elements from the edge or face. A growth rate of 1.05 results in a 5% increase in element edge length with each succeeding layer of elements.
As reported in Table 2, in order to obtain the aforementioned mesh properties, a smaller distance is imposed between edges on the buildings boundary; otherwise the constraint is relaxed on the rest of the boundaries. The maximum element size is set to assure that every region of the domain is sufficiently refined. Finally, the default value of the growth rate 1.2 is decreased to 1.05, this leading to a slower variation in element size. In the low-rise case, the number of nodes is equal to 19111, whereas in the high-rise case is 144663. This last fact will inevitably lead to an higher computational time for the second scenario. In Figure 4 and Figure 5 we report the meshes obtained with the previous domains and parameters.

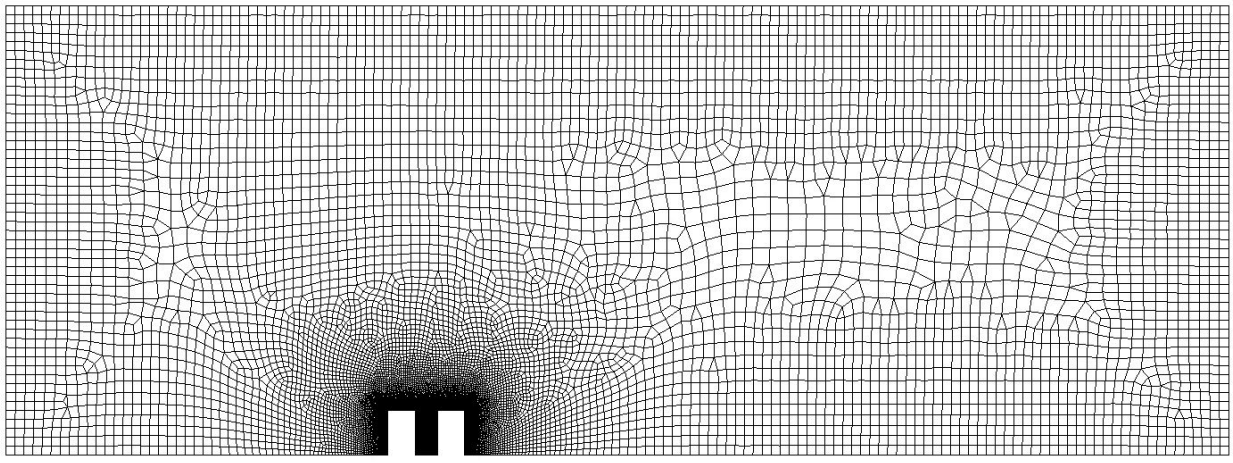

Figure 4: Low-rise mesh (19111 nodes).

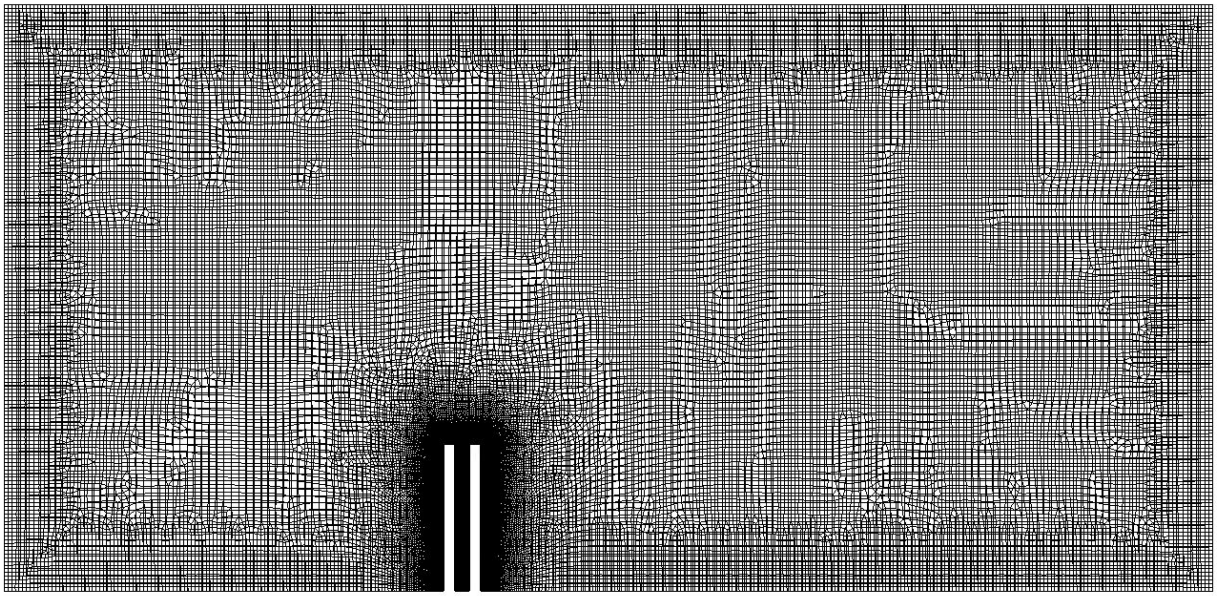

Figure 5: High-rise mesh (144663 nodes).

2 Mathematical formulation and boundary conditions

Considering the 2D assumption, the system of equations to be solved reduces to:

$$\begin{cases} \dfrac{\partial u}{\partial x} + \dfrac{\partial v}{\partial y} = 0 \\ u\dfrac{\partial u}{\partial x} + v\dfrac{\partial u}{\partial y} = -\dfrac{1}{\rho}\dfrac{\partial p}{\partial x} + \nu\left(\dfrac{\partial^2 u}{\partial x^2} + \dfrac{\partial^2 u}{\partial y^2}\right) \\ u\dfrac{\partial v}{\partial x} + v\dfrac{\partial v}{\partial y} = -\dfrac{1}{\rho}\dfrac{\partial p}{\partial y} + \nu\left(\dfrac{\partial^2 v}{\partial x^2} + \dfrac{\partial^2 v}{\partial y^2}\right) \end{cases}$$

where u is the horizontal velocity, v the vertical velocity, p the pressure, ρ the density of the fluid and ν the kinematic viscosity. The approach of Reynolds-averaged Navier Stokes equations (RANS) is used to deal with the turbulent flow regime of this case study. RANS equations can be obtained from the general form of the Navier Stokes equations shown above using Reynolds decomposition. In this way, the steady-state solution is decoupled from the time-varying fluctuations in the system, the latter of which will account for turbulence and will be modeled through a turbulence model presented in the third paragraph. Moreover, in order to solve the system, boundary conditions are necessary.

2.1 Boundary conditions

Boundary conditions are essential in order to define a problem, as well as in computational fluid dynamics. This is not only to achieve the mathematical closure of the system but also to reflect the realistic phenomenon in the most accurate and simple way. The applied boundary conditions are illustrated in the next paragraphs.

Upstream edge: velocity inlet

For turbulent boundary layers over rough surfaces, such as the atmospheric boundary layer of our case study, the typical velocity profile is a Logarithmic Velocity Profile [2]. For this reason, this kind of profile is imposed for the wind velocity at the inlet of our domain (i.e. the left edge of the domain). The resulting inlet velocity function is:

$$\vec{v}_{inlet}(y) = \frac{u^*}{k}\log\left(\frac{y-d}{z_0}\right)\vec{e}_x$$

In particular, we set the friction velocity $u^* = 0.35$ and the aerodynamic roughness length $z_0 = 0.0005$. k is the *Von-Karman* constant ($k = 0.42$) and d is the height shift, in this case 0. Please note that z_0 is scaled by 100 and thus it corresponds to the aerodynamics roughness of 0.05 of the real dimensions case. In particular, this is the tabulated value for crop fields, which could be the cultivation present in the city outskirts. Finally, u^* is chosen in such a way to have a wind velocity of around 4.5 m/s at 1 meter from the ground. This value represents a moderate wind velocity.

Downstream edge: pressure outlet

When a flow rate is imposed at the inlet, a pressure outlet boundary condition is typically used, *i.e.* pressure is fixed and velocity gradient is set to 0, because the flow attains a fully developed state where no change occurs in the flow direction. In these simulations, the Gauge Pressure, the pressure relative to atmospheric pressure, is set to the default value 0.

Top edge: symmetry condition

A symmetry boundary condition is applied at the top of the domain, so that the expected flow field pattern of the developed solution is mirrored along this boundary. In particular, no flow and no scalar flux are imposed across boundary. This is consistent with the realistic phenomenon: due to the horizontal inlet and the long distance from the buildings, the flow velocity is expected to be almost completely horizontal.

Floor and buildings: wall condition

Aside from the street, buildings and floor represent the only solid surfaces; they cause friction and air cannot pass through them. Hence, a wall condition is imposed on these boundaries; in other terms, the wind velocity is almost zero very close to the wall (this is referred to as *no-slip* condition).

Street: pollution inlet

As previously mentioned, pollution is coming from vehicles in transit on the road. Thus the pollution source must be located at the center of the boundary edge between the two buildings and sidewalks should not be considered as source of pollution. The pollution inlet velocity is modeled with only the vertical component different from 0 and the profile has been set through a user-defined function such that the returned value is uniform in the central interval (*i.e.* the street), zero otherwise (*i.e.* the sidewalks). Moreover, the emission of pollutant is simulated only in the interval $[0, T]$, where T is fixed. In this way, the pollutant dispersal is simulated after the emission instead of having an unrealistic constant and infinite-long inlet velocity. For instance, this could represent what happens at night. To obtain the desired result, a step-size function is used, as can be seen from the code implemented for the low-rise domain (Listing 1). An analogous code has been implemented for the high-rise case.

Listing 1: User-defined function for pollutant inlet (low-rise case).

```
#define U 0.06 // Velocity intensity
#define ground_left 4.25 // length of the floor at the left of buildings
#define x_building 0.3  // width of buildings
#define total_street 0.25 // total length of street (including sidewalks)
#define footpath 0.05 // sidewalk length
#define T 1.0 // interval of time for pollutant emission

DEFINE_PROFILE(y_velocity,t,i)
{
real y, x[ND_ND];
real flow_time = CURRENT_TIME;
face_t f;

begin_f_loop(f,t)
{
F_CENTROID(x,f,t);
```

```
y = x[0];
if (t > T)
    F_PROFILE(f,t,i) = 0; // out of the emission time interval
else if (y <= ground_left + x_building + footpath)
    F_PROFILE(f,t,i) = 0; // on the left sidewalk
else if (y >= ground_left + x_building + total_street - footpath)
    F_PROFILE(f,t,i) = 0; // on the right sidewalk
else
    F_PROFILE(f,t,i) = U; // on the street
}
end_f_loop(f,t)
}
```

3 Models and numerical methods

3.1 Turbulence models

In order to solve the system of equations, Reynolds Averaged Navier Stokes (RANS) method is applied. In particular, what is solved is the mean flow field, while all the turbulent scales are modelled. Then, RANS simulations correspond to substantially lower computational costs compared to DNS and LES, but they are highly sensitive to the choice of turbulence model. The possible turbulence models to be adopted could be the standard $k-\epsilon$ ([3]) or $k-\omega$ ([4],[5]), but also the improved Re-Normalisation Group (RNG) $k-\epsilon$ ([6]), Shear-Stress Transport (SST) $k-\omega$ ([7]) and SST γ-Re_θ ([8],[9]). A comprehensive comparison of these models in an urban environment has already been done in [10], in which it is reported a relatively better performance of the SST $k-\omega$ and SST γ-Re_θ models in both unstructured and coarse grid resolution. In particular, solutions obtained with different turbulent models were compared both to a reference wind tunnel experiment and a LES simulation. For this reason, the turbulence model chosen for our project is SST $k-\omega$. This model is a hybrid model combining the $k-\omega$ and $k-\epsilon$ models. It uses a blending function (F_2) to activate the $k-\omega$ model near the wall and the $k-\epsilon$ model in the freestream. This is obtained by modifying the definition of ν_t such that:

$$\nu_t = \min\left\{\frac{k}{\omega}, \frac{ak}{SF_2}\right\},$$

$$F_2 = \tanh\left(\Phi_2^2\right),$$

$$\Phi_2 = \max\left\{2\frac{\sqrt{k}}{0.09\omega y}, \frac{500\mu}{\rho y^2 \omega}\right\},$$

where a is a constant and S is the strain rate magnitude. This choice revealed to be suitable for this problem and settings. However, further studies may investigate the 2-dimensional urban canyon with the adoption of other turbulence models.

3.2 Pollutant model

As already introduced, our problem deals with the supply of pollutant air that originates at the street level. We have already shown that this boundary is considered, for simplicity, as a velocity inlet of pollutant air with constant but limited in time, uniform and vertical velocity from the street edge excluding the sidewalks. The differences with the mean velocity inlet are then the definition of the inlet function and the kind of air mixture that is supplied in inlet. To resemble the realistic case, the pollutant substance that has been chosen is "Diesel-air", already provided by Ansys®. In order to set its composition, we referred to the so-called *air-fuel ratio* that, for Diesel motors, is to be considered approximately 14.7 ([11]), *i.e.* the ratio between air and fuel concentrations. The remaining concentrations come from the air standard composition. In Table 3, the resulting composition of the pollutant mixture is reported.
To conclude, the street inlet velocity has been set to $0.06\,m/s$, a fair value to represent the upward wind velocity in urban cities as shown in [12].

Substance	Name	Concentration
$C_{10}H_{22}$	Decane	6.4%
N_2	Nitrogen	73.0%
O_2	Oxigen	19.6%
CO_2	Carbon dioxide	1.0%

Table 3: Pollutant mixture composition at inlet.

3.3 Numerical methods

For what concerns the spacial discretization, a second-order scheme has been used for all the components. In particular, a second-order upwind scheme [13] has been adopted for the momentum, turbulent kinetic energy and specific dissipation rate.
Instead, for the pressure-velocity coupling, suggested alternating methods such as SIMPLE, SIMPLER, SIMPLEC methods [14] have been avoided preferring a much more demanding but robust coupled scheme. It indeed requires more computational time per iteration but, on the other hand, it is faster and always guarantees convergence. Lighter alternating schemes, instead, did not converge in a few simulations hanging in periodic oscillations. To see in details the adopted coupled scheme, we refer to the Ansys® documentation.

4 Results

In the next paragraphs the simulations results are presented. In particular, in subsection 4.1 the focus is on the simulation of the wind flow in urban environment, whereas in subsection 4.2 the pollutant inlet has been added.

4.1 Wind flow analysis

In Figure 6, the velocity magnitude contours are shown. The arrows also represent the velocity direction and intensity. In the low-rise scenario, velocity ranges between 0 and around 9 m/s; in the other scenario instead, velocity reaches almost 15 m/s. This is explained by the higher height of the second domain. In agreement with the theoretical results, a logarithmic profile is visible on the upstream edge of the domain. However, when the flow reaches the buildings, it is necessarily deflected and the contours reveal a wind acceleration over the obstacles and a low velocity wake behind them, with the separation point positioned at the left vertex of the block. In both cases, it is the part of the domain occupied by the wake that is subject to turbulence, as can be seen from the turbulence kinetic energy in Figure 7.
Regarding the difference in the two configurations, in the high-rise scenario, the wake is longer and more expanded, since its sourcing point is higher. In general, as one should expect, the flow is largely modified by these settings, whereas the lower the buildings the lower the impact on the wind pattern.
This is also what happens to pressure (Figure 8). In both cases, the first building originates a negative relative pressure zone behind himself and the whole downstream area is affected; however, in the high rise scenario, the pressure alteration is much more extensive.

Focusing on the buildings block surrounding area, some characteristics needs to be reported for both the scenarios (Figure 9). First, due to the wall condition and the spanwise direction of the street, the wind velocity is reduced to a maximum of 1 m/s around the block. Secondly, the left wall of the first building causes two separated zones: the former at the bottom-left of the wall, where a clockwise vortex is triggered as the flow is deflected downward; the latter at the top-left of the wall, where the flow is deflected upward and then accelerated.

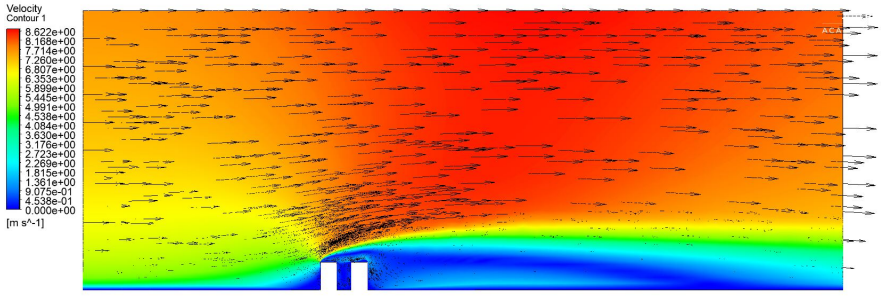

(a) Low-rise solution.

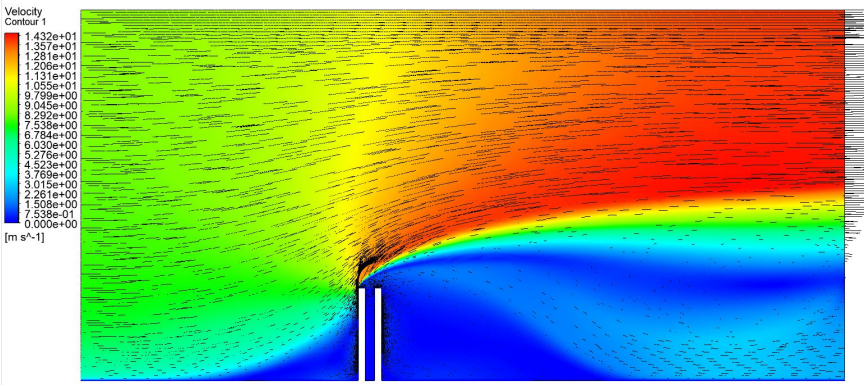

(b) High-rise solution.

Figure 6: Full domain velocity contour plots.

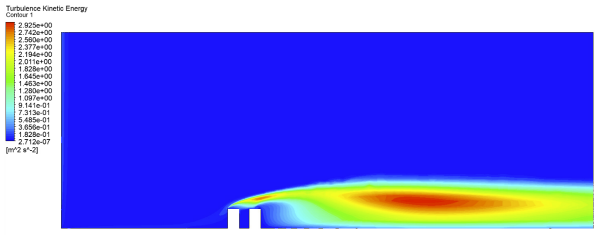

(a) Low-rise solution.

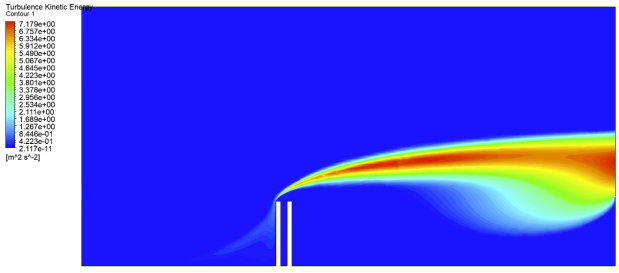

(b) High-rise solution.

Figure 7: Full domain turbulence kinetic energy contour plots.

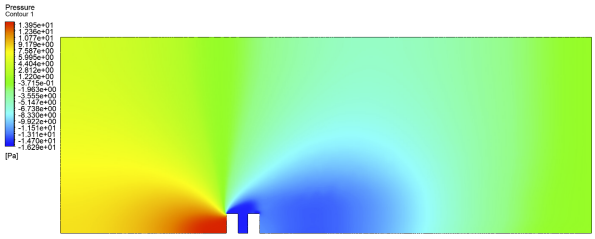

(a) Low-rise solution.

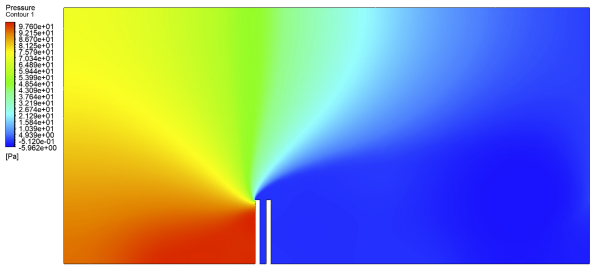

(b) High-rise solution.

Figure 8: Full domain pressure contour plots.

In addition, two other vortexes are discernible. A clockwise swirl is the already mentioned wake on the downstream side of the block. Moreover, due to the presence of the wake, the wind blows leftward at the top of the buildings originating an anticlockwise vortex in the canyons. Here, the two simulations need to be compared. In the low-rise case, the vortex fill the whole space between the buildings; instead, in the high-rise case, the vortex is located only on the top part of the canyon, because of the extremely tall height of these buildings. This causes a practically nonexistent recirculation on the lower part of the canyon. As further discussed in subsection 4.2, this will lead to different behaviour of the pollutant transport.
As a last note, especially in the first case, the right wall of the block generates the same speed up phenomenon as the left one; in addition, the lower wind velocity allows the flow to reattach on the building rooftop itself.

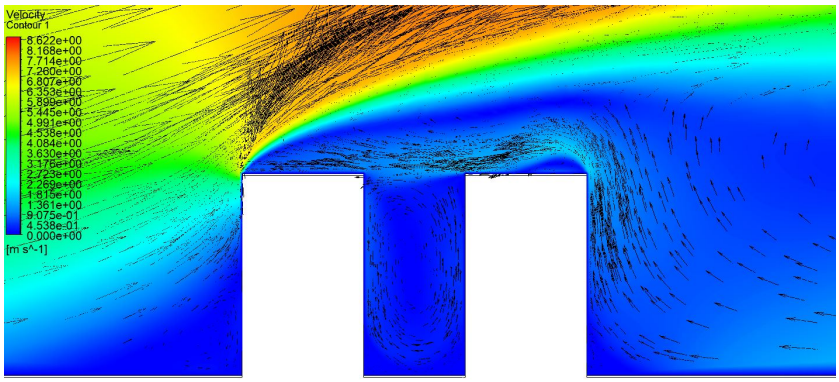

(a) Low-rise solution.

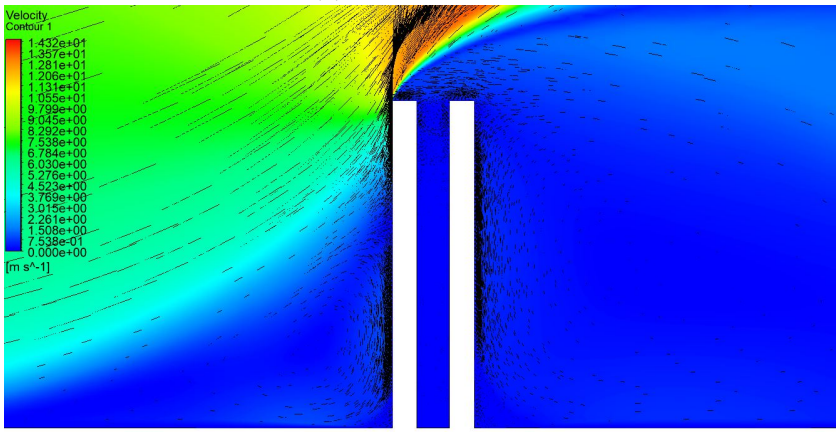

(b) High-rise solution.

Figure 9: Buildings velocity contour plots.

4.2 Pollutant dispersion analysis

In Figure 10, the pollutant dispersion contours are shown; the colors represent the concentration of decane ($C_{10}H_{22}$), while the arrows the direction and intensity of the wind velocity. Here the role of the street canyon vortexes is evident. In the low-rise case, the swirl is able to move part of the mixture upward and, due to the anticlockwise direction, more pollutant is indeed found on the right side of the canyon. On the other hand, in the second plot, the pollutant transport is due only to diffusive effects. Precisely, there are color separations that may hint at the presence of some eddies but, in any case, they have very weak intensities.

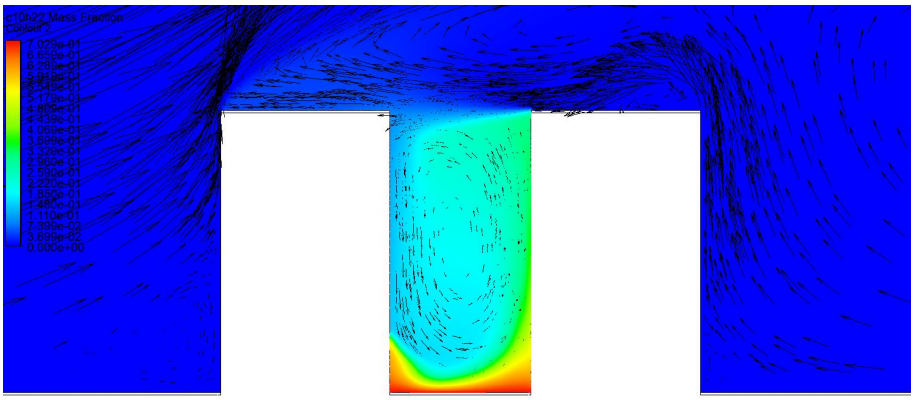

(a) Low-rise solution.

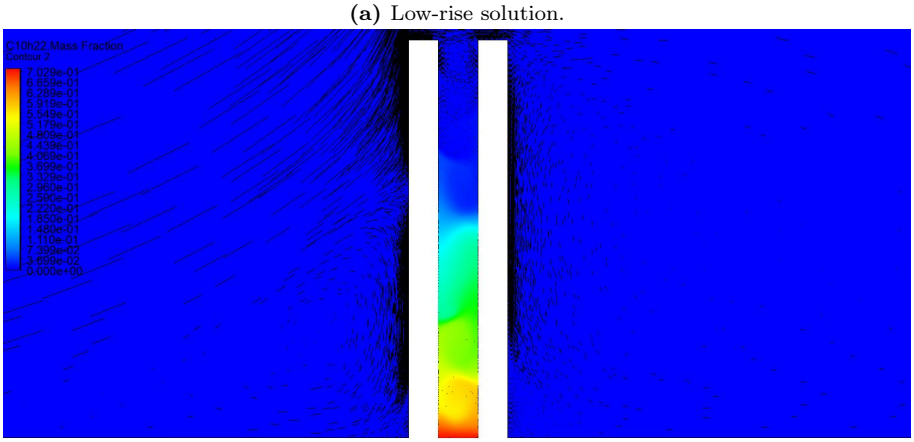

(b) High-rise solution.

Figure 10: Pollutant concentration contour plots.

However, because of the two different length scales, the comparison is not always self-explanatory and the plots in Figure 11 could help the analysis. A measurement of the pollutant concentration and the velocity curl has been done along the symmetry vertical line between the two buildings. The pollutant layer in the low-rise simulation is actually very thin ($\approx 5\,m$) while, in the other scenario, more than $150\,m$ are required to reach the same low level of pollutant (Figure 11a). Moreover, the vortex effect can be deduced from the non-monotonicity of the two lines: in the low-rise case, the effect is significant and causes the increment of the concentration in the whole interval $0 - 50\,m$. In the high-rise case there are some little oscillations that, as for the color separation previously discussed, hint at the presence of multiple but weak vortexes.
Finally, the intensity of the vortexes is confirmed by Figure 11b where the low-rise simulation presents an almost constant value ($\approx 5\ S^{-1}$) of velocity curl through the whole canyon. On the contrary, the vorticity of the second solution is negligible. These observations are referred to the behaviour inside the canyon: on the street and on top other phenomena need to be considered.

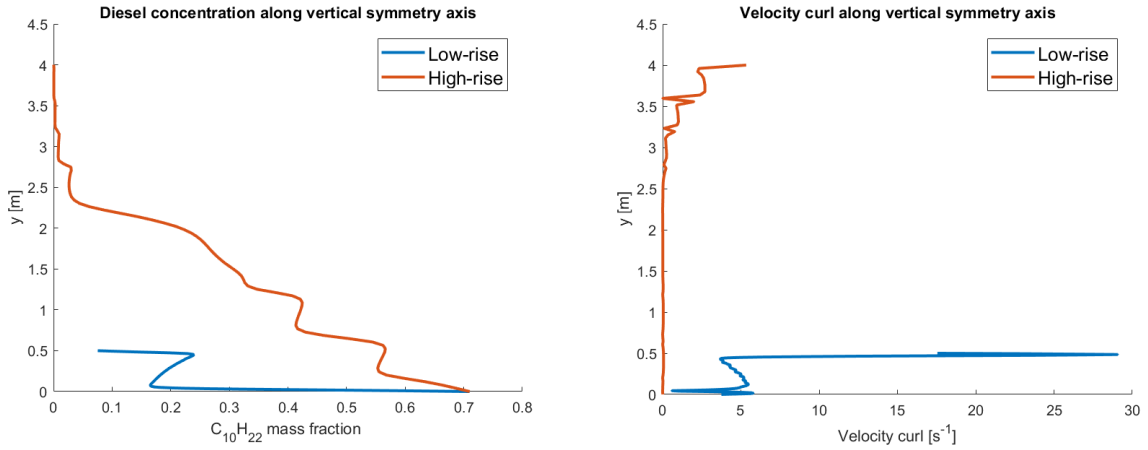

(a) Pollutant concentration.

(b) Velocity curl.

Figure 11: Comparison of pollutant concentration and velocity curl along the symmetry vertical axis.

5 Conclusions

From the results shown in the previous sections, the main differences between the two scenarios can be highlighted. Summing up, in the low-rise simulation, a canyon vortex with mild intensity is present and covers almost all the canyon area. Due to friction with the solid ground, there is a thin layer on the street level where the vortex has not sufficient intensity and pollutant is stagnant. On the other hand, in the high-rise simulation, a vortex with low intensity covers only the very upper part of the canyon and, in almost all the canyon area, there are multiple but weak vortexes. The pollutant is here stagnant everywhere and it moves upward slowly, mainly thanks to weak diffusive effects.
A practical solution for the first scenario could be found in the following reasoning. Since approximately only the first $5\,m$ of layer is stagnant, it could be then sufficient to move upward only the pollutant at the street level. For instance, some turbines may be placed on the ground and the upward transport of only few meters could be enough for a complete pollutant circulation. On the other hand, no feasible solution could be deduced from our results in very urban cities. Here, there is no wind contribution that can help the human resources and the artificial transportation of pollutant for hundreds of meters is not practicable.
Finally, some limitations of the present work need to be stressed. First, only one canyon has been considered, this being far from representing a whole city. Secondly, also different ratios between left and right building heights could provide different results. Furthermore, the 2D assumption makes sense only with an infinite long street, hence an unrealistic case. Finally, no thermal effects has been taken into consideration.
Besides the aforementioned flaws of this project, the study of the canyon vortex is valid and highly significant for the pollutant transport, thus a good starting point for further research.

References

[1] Yousef Abu-Zidan, Priyan Mendis and Tharaka Gunawardena. 'Optimising the computational domain size in CFD simulations of tall buildings'. In: *Heliyon* 7.4 (2021). ISSN: 2405-8440. DOI: https://doi.org/10.1016/j.heliyon.2021.e06723.

[2] Ulf Högström. 'Review of some basic characteristics of the atmospheric surface layer'. In: *Boundary-Layer Meteorology* 78 (1996). ISSN: 1573-1472. DOI: 10.1007/BF00120937.

[3] B. E. Launder and D. B. Spalding. 'The numerical computation of turbulent flows'. In: *Computer Methods in Applied Mechanics and Engineering* 3.2 (1974), pp. 269–289. ISSN: 0045-7825. DOI: 10.1016/0045-7825(74)90029-2.

[4] David Wilcox. *Turbulent Modelling for CFD*. Jan. 2004.

[5] David Wilcox. 'Formulation of the k - ω Turbulence Model Revisited'. In: *Aiaa Journal* 46 (Nov. 2008), pp. 2823–2838. DOI: 10.2514/1.36541.

[6] V. Yakhot et al. 'Development of Turbulence Models for Shear Flows by a Double Expansion technique'. In: *Physics of Fluids A Fluid Dynamics* 4 (Aug. 1992), pp. 1510–1520. DOI: 10.1063/1.858424.

[7] F. R. Menter. 'Zonal Two Equation k-ω Turbulence Models for Aerodynamic Flows'. In: *AIAA Fluid Dynamics Conference* 93-2906 (1993). DOI: 10.2514/6.1993-2906.

[8] F. R. Menter, R. Langtry and S. Volker. 'Transition Modelling for General Purpose CFD Codes'. In: *Flow, Turbulence and Combustion* 77 (2006), pp. 277–303. DOI: 10.1007/s10494-006-9047-1.

[9] R. Langtry and F. R. Menter. 'Correlation-Based Transition Modeling for Unstructured Parallelized Computational Fluid Dynamics Codes'. In: *AIAA Journal* 47 (2009), pp. 2894–2906. DOI: 10.2514/1.42362.

[10] Farshid Kardan, Olivier Baverel and Fernando Porté-Agel. 'Assessment of RANS Turbulence Models in Urban Environments: CFD Simulation of Airflow Around Idealized High-Rise Morphologies'. In: *Humanizing Digital Reality* (Sept. 2018), pp. 259–269. DOI: 10.1007/978-981-10-6611-5_23.

[11] Qianfan Xin. *Diesel Engine System Design*. Sawston: Woodhead Publishing, 2011. ISBN: 9780081016916.

[12] Van Thinh Nguyen, Thanh Chuyen Nguyen and John Nguyen. 'Numerical Simulation of Turbulent Flow and Pollutant Dispersion in Urban Street Canyons'. In: *Atmosphere* 10.11 (2019). ISSN: 2073-4433. DOI: 10.3390/atmos10110683.

[13] Charles Hirsch. *Numerical Computation of Internal and External Flows*. New York: John Wiley Sons, 1990. ISBN: 978-0-471-92452-4.

[14] Edouard Audi. 'Comparison of pressure-velocity coupling schemes for 2D flow problems'. In: *International Conference on Advances in Computational Tools for Engineering Applications* (2009), pp. 245–248. DOI: 10.1109/ACTEA.2009.5227833.